Multibody System Dynamics **6:** 245–266, 2001.

A Perturbation Method for Dynamic Analysis and Simulation of Flexible Manipulators

J.B. JONKER and R.G.K.M. AARTS
Department of Mechanical Engineering, University of Twente, P.O. Box 217, 7500 AE Enschede, The Netherlands; E-mail: J.B.Jonker@wb.utwente.nl; R.G.K.M.Aarts@wb.utwente.nl

(Received: 5 November 1999; accepted in revised form: 18 October 2000)

Abstract. This paper presents a perturbation method for the dynamic simulation of flexible manipulators. In this method the vibrational motion of the manipulator is modeled as a first-order perturbation of the nominal rigid link motion. For that purpose the flexible dynamic model is split into two parts. A rigidified system describes the nominal rigid link motion of the manipulator. A linear system linearized about the nominal trajectory describes the vibrational motion. These equations are computationally more efficient than the non-linear dynamic equations and offer more insight in the dynamic phenomena of the system. The method is based on a full non-linear finite element formulation which treats the general case of coupled large displacements motion and small elastic motion. A planar one link manipulator and a spatial two link manipulator with flexible links are used for case studies. A comparison is made between the non-linear and the perturbation analyzes. The perturbation method appears to be a very efficient approach for dynamic analyzes of flexible manipulators and yields accurate results even for systems with low frequency elastic modes.

Key words: finite element modeling, perturbation method, SPACAR/SIMULINK interface, flexible manipulator, closed-loop trajectory control.

1. Introduction

Dynamic simulation of flexible manipulators is a crucial part in the design of manipulators where the combination of high speed and precision is essential. The dynamic equations of flexible manipulators are highly non-linear and have a large dimension, especially when high frequency elastic modes have to be considered. The non-linearities are due to the large relative displacements and rotations between the links whereas the large dimension of the system arises from the large number of flexible degrees of freedom necessary to describe the elastic modes. For the purpose of control system design it is desirable to represent the dynamic equations in terms of a mixed set of generalized coordinates of the manipulator with rigid links which are used for describing control forces and torques, and deformation coordinates that characterize flexible deformations. This formulation, however, suffers from computational drawbacks due to the requirement for an iterative solution of the dependent generalized coordinates. This makes the simulation computationally very

expensive and time consuming. In addition a non-linear simulation result does not necessarily provide an insight into the complex interactions of the system.

In many cases the non-linearity is mainly restricted to the slow dynamics associated with the gross manipulator motion. The fast dynamics is represented as the vibrational motion which may be approximated by a linear system with time-varying coefficients. In view of these observations a perturbation formulation for flexible manipulators is derived here, where the fast variables are the elastic degrees of freedom. Using this approach, the elastic motions are computed separately from the rigid link manipulator motion. The rigid link motion is computed first and is described by the rigidified manipulator model, that is a model in which all flexible deformation coordinates are prescribed zero. Next the vibrational motion is described by a set of linear time-varying equations of motion obtained by linearization of the equations of motion around a number of points of the nominal trajectory. From the preceding rigid link dynamic analysis generalized stress resultants of the rigidified links are computed and subsequently applied as excitation forces in solving the linearized equations of motion for elastic vibrations. In this analysis it is assumed that the elastic motion does not influence the rigid link motion.

The methodology could be compared to earlier published superposition methods [1–7], but is actually an application of singular perturbation theory [8, 9]. The method is based on a non-linear finite element method and utilizes an analytical procedure for the generation of the linearized equations of motion. The analytical approach leads to a system of linearized equations in which the matrix coefficients possess all dynamical properties of the system. This offers a profound insight into the dynamic and geometric stiffening effects on the vibrational motion. The perturbation scheme is used for dynamic simulations of flexible link manipulators including the effects of the manipulator's control system. The control algorithm employed consists of an open-loop and a closed-loop part. The open-loop control produces the desired overall rigid link motion, while the feedback control must stabilize and damp the elastic vibrations which are naturally excited by the rigid link motion.

The proposed perturbation method applies for both planar as well as spatial flexible manipulators with revolute and translational joints and is implemented in the program SPACAR [10]. An interface to MATLAB is available and simulations are carried out using SIMULINK's [11] graphical user interface. The applicability of the method is demonstrated by analyzing the open-loop and closed-loop behavior of a flexible one link manipulator example introduced by Kane et al. [12]. Furthermore the closed loop behavior of a 3D flexible manipulator is analyzed. Results obtained using the perturbation method are compared with those obtained from non-linear simulations.

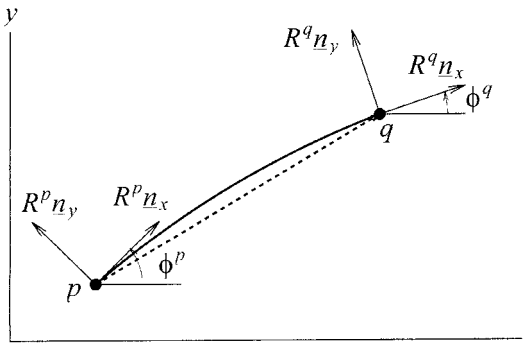

Figure 1. Planar flexible beam element.

2. Finite Element Representation of Manipulators

In the presented finite element method a manipulator mechanism is modeled as an assembly of finite elements interconnected by joint elements such as hinge elements and (slider) truss elements. The manipulator links are modeled by beam elements. The location of each element is described relative to a fixed inertial coordinate system by a set of nodal coordinates $x_i^{(k)}$. Some coordinates may be Cartesian coordinates of the end nodes, while others describe the orientation of orthogonal base vectors or triads, rigidly attached to the element nodes. The superscript k is added to show that a specific element k is considered. With respect to some reference configuration of the element, the instantaneous values of the nodal coordinates represent a fixed number of deformation modes for the element. The deformation modes are specified by a set of deformation parameters $e_i^{(k)}$, some of which are associated with large relative displacements and rotations between the element nodes, while others describe small elastic deformations of the element and will be denoted by $\varepsilon_i^{(k)}$. The number of deformation parameters is equal to the number of nodal coordinates minus the number of degrees of freedom of the element as a rigid body. Note that rigid body motions of the elements are characterized by displacements and rotations of the nodal points for which all deformations are zero. The components of the vector of deformation parameters $(\underline{e}^{(k)}, \underline{\varepsilon}^{(k)})$ can be expressed as analytic functions of the vector of nodal coordinates $\underline{x}^{(k)}$. In this way we can define for each element k a vector function $(\underline{e}^{(k)}, \underline{\varepsilon}^{(k)}) = \underline{\mathcal{D}}^{(k)}(\underline{x}^{(k)})$.

2.1. PLANAR BEAM ELEMENT

As a first example the deformation functions $\mathcal{D}_i^{(k)}$ of the planar beam element are presented. The configuration of a beam element is defined by the position vectors $\underline{x}^p$ and $\underline{x}^q$ of the end nodes p and q and the angular orientation of orthonormal base vectors $(R^p\underline{n}_x, R^p\underline{n}_y)$ and $(R^q\underline{n}_x, R^q\underline{n}_y)$ rigidly attached to the element nodes as shown in Figure 1.

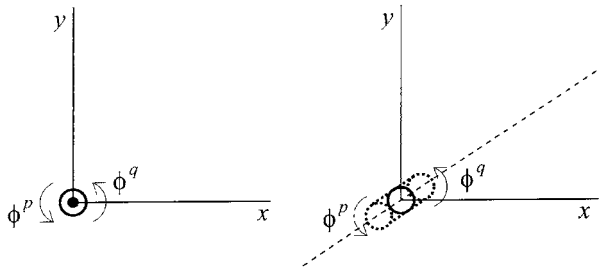

Figure 2. The planar hinge element.

The rotation part of the motion of the beam element is described by the planar rotation matrices R^p and R^q. The nodal coordinates of the beam element are four Cartesian coordinates (x^p, y^p), (x^q, y^q) describing the position of the beam in the (x, y)-coordinate system and two rotation angles ϕ^p and ϕ^q representing the angular orientation of the base vectors $(R^p\underline{n}_x, R^p\underline{n}_y)$ and $(R^q\underline{n}_x, R^q\underline{n}_y)$ at the nodes p and q respectively. Hence the vector of nodal coordinates is given by

$$\underline{x}^{(k)}_{\text{beam}} = \left[x^p, y^p, \phi^p \mid x^q, y^q, \phi^q\right]^T . \tag{1}$$

The number of degrees of freedom of the element as a rigid body is three, which gives rise to three elastic deformation parameters. Deformation $\varepsilon_1^{(k)}$ represents the elongation of the element and two deformation mode coordinates $\varepsilon_2^{(k)}$ and $\varepsilon_3^{(k)}$ are associated with the flexible deformation of the beam element. A proper definition of deformations requires that the deformation parameters are invariant under rigid body movements of the element. This condition is satisfied by defining

$$\begin{aligned}
\text{elongation:} \quad \varepsilon_1^{(k)} &= ||\underline{l}^{(k)}|| - l_0^{(k)} \\
&\quad + \frac{1}{30 l_0^{(k)}}\left[2(\varepsilon_2^{(k)})^2 + \varepsilon_2^{(k)}\varepsilon_3^{(k)} + 2(\varepsilon_3^{(k)})^2\right], \\
\text{bending:} \quad \varepsilon_2^{(k)} &= -(R^p\underline{n}_y, \underline{l}^{(k)}), \\
\varepsilon_3^{(k)} &= (R^q\underline{n}_y, \underline{l}^{(k)}),
\end{aligned} \tag{2}$$

where $l_0^{(k)}$ is the reference length of the element and the vector $\underline{l}^{(k)}$ is defined by

$$\underline{l}^{(k)} = \underline{x}^q - \underline{x}^p = [x^q - x^p, y^q - y^p]^T. \tag{3}$$

Note that in the expression for the elongation $\varepsilon_1^{(k)}$ second order geometric terms are included representing additional elongation of the beam axis caused by bending [13]. The deformation parameters in Equations (2) possess the proper invariance with respect to rigid body motions of the beam element.

2.2. PLANAR HINGE ELEMENT

The second example is the planar hinge element which can be used to describe the relative angle between two beam elements (Figure 2). The vector of nodal coordinates is

$$\underline{x}_{\text{hinge}}^{(k)} = \left[\phi^p, \phi^q\right]^T, \tag{4}$$

where p and q are the nodes at both sides of the hinge. The deformation mode is the relative rotation angle $e_1^{(k)}$ defined as

$$e_1^{(k)} = \phi^q - \phi^p. \tag{5}$$

2.3. SPATIAL ELEMENTS

For 3D manipulators spatial beam and hinge elements are available. The two end points of a flexible beam element have twelve coordinates. The number of degrees of freedom of the element as a rigid body is six, so there are six elastic deformation parameters: One longitudinal deformation, one torsional deformation and four bending deformations. For a detailed description of deformation functions of the spatial beam and hinge elements the reader is referred to [14, 15].

3. Equations of Motion

A manipulator model can be build up with finite elements by letting them have nodal points in common. The assemblage of finite elements is realized by defining a vector $\underline{x}$ of nodal coordinates for the entire manipulator mechanism. The deformation functions of the element can be described in terms of the components of $\underline{x}$. The equations can be written as

$$\begin{bmatrix} e_1 \\ \vdots \\ e_{ne} \\ \varepsilon_{ne+1} \\ \vdots \\ \varepsilon_{ne+n\varepsilon} \end{bmatrix} = \begin{bmatrix} \mathcal{D}_1(\underline{x}) \\ \vdots \\ \mathcal{D}_{ne}(\underline{x}) \\ \mathcal{D}_{ne+1}(\underline{x}) \\ \vdots \\ \mathcal{D}_{ne+n\varepsilon}(\underline{x}) \end{bmatrix}, \tag{6}$$

or

$$\begin{bmatrix} \underline{e} \\ \underline{\varepsilon} \end{bmatrix} = \begin{bmatrix} \underline{\mathcal{D}}^{(e)}(\underline{x}) \\ \underline{\mathcal{D}}^{(\varepsilon)}(\underline{x}) \end{bmatrix}, \tag{7}$$

where ne and $n\varepsilon$ are the total number of deformation parameters of the mechanism associated with large relative displacements and rotations and with small

elastic deformations, respectively. The kinematic constraints can be introduced by putting conditions on the nodal coordinates $\underline{x}$ as well as by imposing conditions on the deformation parameters $(\underline{e}, \underline{\varepsilon})$ which are all assumed to be holonomic. A frequently used mathematical model of a manipulator mechanism is the model in which all elastic deformations of the links are neglected. According to Equation (7) the motion of the manipulator is then restricted to motions for which $\underline{\varepsilon} = \underline{0}$.

The motion of manipulator mechanisms is described by relative degrees of freedom, which can be either actuator joint coordinates, denoted $\underline{e}^m$, as well as elastic deformation parameters denoted by $\underline{\varepsilon}^m$. The superscript m is used to denote the degrees of freedom. The objective of kinematic analysis is to solve system (7) for the vector of generalized coordinates $\underline{q} = (\underline{e}^m, \underline{\varepsilon}^m)^T$. The solution is expressed by means of a geometric transfer function $\underline{\mathcal{F}}$ as

$$\underline{x} = \underline{\mathcal{F}}(\underline{e}^m, \underline{\varepsilon}^m) = \underline{\mathcal{F}}(\underline{q}). \tag{8}$$

Generally this transfer function cannot be calculated explicitly from the constraint equations (7) but has to be determined numerically in an iterative way [10].

The inertia properties of the concentrated and distributed mass of the elements are described with the aid of lumped and consistent mass matrices [14–16]. Let $M(\underline{x})$ be the global mass matrix, obtained by assembling the lumped and consistent element mass matrices, and let $\underline{f}(\underline{x}, \dot{\underline{x}}, t)$ be the vector of nodal forces, including the velocity dependent inertia forces. The loading state of each element is described by a vector of stress resultants. The vectors are assembled in the global vectors $\underline{\sigma}^e$ and $\underline{\sigma}^\varepsilon$, dual to $\dot{\underline{e}}$ and $\dot{\underline{\varepsilon}}$, respectively. According to the principle of virtual power for the external forces including the inertial forces and stress resultant vectors $\underline{\sigma}^{em}$ and $\underline{\sigma}^{\varepsilon m}$ of the manipulator mechanism, we obtain

$$\left\langle (\underline{f} - M\ddot{\underline{x}}), \delta\dot{\underline{x}} \right\rangle = \left\langle (\underline{\sigma}^{em}, \underline{\sigma}^{\varepsilon m}), (\delta\dot{\underline{e}}^m, \delta\dot{\underline{\varepsilon}}^m) \right\rangle, \tag{9}$$

for all virtual velocities $\delta\dot{\underline{x}}$, which satisfy all instantaneous kinematic constraints. By differentiating the transfer function (8), we obtain

$$\dot{\underline{x}} = \frac{\partial \underline{\mathcal{F}}}{\partial \underline{e}^m}\dot{\underline{e}}^m + \frac{\partial \underline{\mathcal{F}}}{\partial \underline{\varepsilon}^m}\dot{\underline{\varepsilon}}^m. \tag{10}$$

Using the differentiation operator D to represent partial differentiation with respect to the vector of the degrees of freedom, we write for Equation (10)

$$\dot{\underline{x}} = \mathrm{D}\underline{\mathcal{F}} \cdot (\dot{\underline{e}}^m, \dot{\underline{\varepsilon}}^m), \tag{11}$$

and for the second derivative

$$\ddot{\underline{x}} = (\mathrm{D}^2\underline{\mathcal{F}} \cdot (\dot{\underline{e}}^m, \dot{\underline{\varepsilon}}^m)) \cdot (\dot{\underline{e}}^m, \dot{\underline{\varepsilon}}^m) + \mathrm{D}\underline{\mathcal{F}} \cdot (\ddot{\underline{e}}^m, \ddot{\underline{\varepsilon}}^m). \tag{12}$$

Substitution of Equation (12) in the virtual power equation (9) yields the reduced equations of motion

$$\begin{bmatrix} \bar{M}^{ee} & \bar{M}^{e\varepsilon} \\ \bar{M}^{\varepsilon e} & \bar{M}^{\varepsilon\varepsilon} \end{bmatrix} \begin{bmatrix} \ddot{\underline{e}}^m \\ \ddot{\underline{\varepsilon}}^m \end{bmatrix} + \begin{bmatrix} \mathrm{D}_{e^m} \underline{\mathcal{F}}^T \\ \mathrm{D}_{\varepsilon^m} \underline{\mathcal{F}}^T \end{bmatrix} \left[M(\mathrm{D}^2 \underline{\mathcal{F}} \cdot (\dot{\underline{e}}^m, \dot{\underline{\varepsilon}}^m)) \cdot (\dot{\underline{e}}^m, \dot{\underline{\varepsilon}}^m) - \underline{f} \right] = - \begin{bmatrix} \underline{\sigma}^{em} \\ \underline{\sigma}^{\varepsilon m} \end{bmatrix}, \tag{13}$$

with the reduced mass matrices:

$$\begin{aligned} \bar{M}^{ee} &= \mathrm{D}_{e^m} \underline{\mathcal{F}}^T M \mathrm{D}_{e^m} \underline{\mathcal{F}}, \qquad \bar{M}^{e\varepsilon} = \mathrm{D}_{e^m} \underline{\mathcal{F}}^T M \mathrm{D}_{\varepsilon^m} \underline{\mathcal{F}}, \\ \bar{M}^{\varepsilon e} &= \mathrm{D}_{\varepsilon^m} \underline{\mathcal{F}}^T M \mathrm{D}_{e^m} \underline{\mathcal{F}}, \qquad \bar{M}^{\varepsilon\varepsilon} = \mathrm{D}_{\varepsilon^m} \underline{\mathcal{F}}^T M \mathrm{D}_{\varepsilon^m} \underline{\mathcal{F}}. \end{aligned} \tag{14}$$

The matrices $\bar{M}^{e\varepsilon}$ and $\bar{M}^{\varepsilon e}$ represent the dynamic coupling between the gross rigid motion and the flexible deformation of the links. The presence of this dynamic coupling is one of the major problems encountered in controlling flexible manipulators. The stress resultant vector of elastic elements is characterized by Hooke's law defined by $\underline{\sigma}^{\varepsilon} = K^{\varepsilon\varepsilon} \underline{\varepsilon}$, where $K^{\varepsilon\varepsilon}$ is a symmetric matrix containing the elastic constants. The driving forces and torques, represented by the vector $\underline{\sigma}^{em}$, are applied only at the actuator joints. If the actuator dynamics are not considered then there is a simple linear relation between the vector of control inputs $\underline{u}$ and the vector $\underline{\sigma}^{em}$

$$\underline{\sigma}^{em} = -\underline{u}. \tag{15}$$

The minus sign in Equation (15) is a result of different sign conventions for the driving forces in control engineering literature and in structural dynamics literature. With Equation (15), Hooke's law and the definition of $\underline{q}$, the equations of motion in (13) can be written in a more compact form

$$\bar{M}(\underline{q}) \ddot{\underline{q}} + \mathrm{D} \underline{\mathcal{F}}^T \left[M(\mathrm{D}^2 \underline{\mathcal{F}} \cdot \dot{\underline{q}}) \cdot \dot{\underline{q}} - \underline{f} \right] + \bar{K} \underline{q} = B \underline{u}, \tag{16}$$

where $\bar{K}$ is the structural stiffness matrix of the manipulator mechanism

$$\bar{K} = \begin{bmatrix} 0 & 0 \\ 0 & K^{\varepsilon\varepsilon} \end{bmatrix}, \tag{17}$$

and B is the input matrix defined by

$$B = \begin{bmatrix} I \\ 0 \end{bmatrix}. \tag{18}$$

4. Linearized Equations of Motion

Given the non-linear equations of motion in Equation (16), consider now small perturbations around the nominal trajectory $(\underline{q}_0, \dot{\underline{q}}_0, \ddot{\underline{q}}_0)$ such that the actual variables are of the form

$$\begin{aligned}
\underline{q} &= \underline{q}_0 + \delta\underline{q},\\
\underline{\dot{q}} &= \underline{\dot{q}}_0 + \delta\underline{\dot{q}},\\
\underline{\ddot{q}} &= \underline{\ddot{q}}_0 + \delta\underline{\ddot{q}},
\end{aligned} \tag{19}$$

where the prefix δ denotes a perturbation and should not be confused with the virtual velocities in Equation (9). Expanding Equations (8) and (11) in their Taylor series expansion and disregarding second and higher order terms results in the linear approximations

$$\begin{aligned}
\delta\underline{x} &= \mathrm{D}\underline{\mathcal{F}}\cdot\delta\underline{q},\\
\delta\underline{\dot{x}} &= \mathrm{D}\underline{\mathcal{F}}\cdot\delta\underline{\dot{q}} + (\mathrm{D}^2\underline{\mathcal{F}}\cdot\underline{\dot{q}}_0)\cdot\delta\underline{q}.
\end{aligned} \tag{20}$$

Linearization of the reduced equations of motion (16) around the nominal trajectory $(\underline{q}_0, \underline{\dot{q}}_0, \underline{\ddot{q}}_0)$, results in

$$\bar{M}_0\delta\underline{\ddot{q}} + C_0\delta\underline{\dot{q}} + (K_0 + N_0 + G_0)\delta\underline{q} = B\delta\underline{u}, \tag{21}$$

where $\bar{M}_0$ is the system mass matrix as in (16), C_0 is the velocity sensitivity matrix, and K_0 denotes the structural stiffness matrix as in (17). N_0 and G_0 are the dynamic stiffening matrix and the geometric stiffening matrix, respectively. $\bar{M}_0$, K_0 and G_0 are symmetric matrices, but C_0 and N_0 need not. These matrices are calculated by Meijaard [16] and Jonker [17]

$$\begin{aligned}
C_0 &= \mathrm{D}\underline{\mathcal{F}}_0^T[\mathrm{D}_{\dot{x}}\underline{f}\,\mathrm{D}\underline{\mathcal{F}}_0 + 2M_0\mathrm{D}^2\underline{\mathcal{F}}_0\cdot\underline{\dot{q}}_0],\\
N_0 &= \mathrm{D}\underline{\mathcal{F}}_0^T[(-\mathrm{D}_x\underline{f} + \mathrm{D}_x M_0\underline{\ddot{x}}_0)\mathrm{D}\underline{\mathcal{F}}_0\\
&\qquad + M_0(\mathrm{D}^2\underline{\mathcal{F}}_0\cdot\underline{\ddot{q}}_0 + (\mathrm{D}^3\underline{\mathcal{F}}_0\cdot\underline{\dot{q}}_0)\cdot\underline{\dot{q}}_0) + \mathrm{D}_{\dot{x}}\underline{f}\,\mathrm{D}^2\underline{\mathcal{F}}_0\cdot\underline{\dot{q}}_0],\\
G_0 &= -\mathrm{D}^2\underline{\mathcal{F}}_0^T[\underline{f} - M_0\underline{\ddot{x}}_0].
\end{aligned} \tag{22}$$

The matrix coefficients are functions of time, since they depend on the nominal position, velocity and acceleration of the manipulator.

5. Perturbation of the Rigid Link Motion with Small Elastic Deformations

According to the perturbation method the equations of motion are separated into a set of non-linear equations for the nominal rigid link motion and a set of linearized equations describing the small elastic motions and deviations from the rigid link motion. The nominal rigid link motion is described by the rigidified model, that is a model in which all elastic deformations are prescribed zero. The rigidified model is calculated by setting $\ddot{\underline{\varepsilon}}^m = \dot{\underline{\varepsilon}}^m = \underline{\varepsilon}^m = \underline{0}$ in Equation (13), yielding

$$\begin{aligned}
\bar{M}_0^{ee}\ddot{\underline{e}}_0^m + \mathrm{D}_{e^m}\underline{\mathcal{F}}_0^T\big[M_0(\mathrm{D}^2\underline{\mathcal{F}}_0\cdot(\dot{\underline{e}}_0^m, \underline{0}))\cdot(\dot{\underline{e}}_0^m, \underline{0}) - \underline{f}\big] &= \underline{u}_0,\\
\bar{M}_0^{\varepsilon e}\ddot{\underline{e}}_0^m + \mathrm{D}_{\varepsilon^m}\underline{\mathcal{F}}_0^T\big[M_0(\mathrm{D}^2\underline{\mathcal{F}}_0\cdot(\dot{\underline{e}}_0^m, \underline{0}))\cdot(\dot{\underline{e}}_0^m, \underline{0}) - \underline{f}\big] &= -\underline{\sigma}_0^{\varepsilon m},
\end{aligned} \tag{23}$$

where $\underline{u}_0$ represents the nominal input necessary to move the rigid link manipulator along the nominal (desired) trajectory. The vector $\underline{\sigma}_0^{\varepsilon m}$ describes the generalized stress resultants (Langrange multipliers) of the rigidified links. These forces are balanced by the internal excitation forces of the vibrational motion of the links. They are therefore added to the right hand side of the linearized equations of motion with reversed sign. The elastic motion is then described by a set of inhomogeneous linear time-varying equations of the form

$$\bar{M}_0 \begin{bmatrix} \delta\ddot{\underline{e}}^m \\ \ddot{\underline{\varepsilon}}^m \end{bmatrix} + C_0 \begin{bmatrix} \delta\dot{\underline{e}}^m \\ \dot{\underline{\varepsilon}}^m \end{bmatrix} + \bar{K}_0 \begin{bmatrix} \delta\underline{e}^m \\ \underline{\varepsilon}^m \end{bmatrix} = \begin{bmatrix} \delta\underline{u} \\ \underline{\sigma}_0^{\varepsilon m} \end{bmatrix}, \tag{24}$$

where $\underline{\varepsilon}^m = \delta\underline{\varepsilon}^m$ as $\underline{\varepsilon}_0^m = 0$, $\bar{K}_0$ is defined as

$$\bar{K}_0 = K_0 + N_0 + G_0 \tag{25}$$

and the vector $\delta\underline{u}$ is the control input vector synthesized at the stage of perturbed dynamics.

Using the perturbation method a reduced set of dynamic equations is formulated which explicitly show the relationship between a prescribed motion $\underline{e}_0^m(t)$ and the driving forces and torques $\underline{u}_0$ for the controlling actuators. The nominal control input is used as feedforward compensation for the gross rigid link motion of the manipulator. The main part of the non-linear dynamic effects due to changes of the manipulator configuration as well as the dynamic coupling between the rigid link modes is predicted and cancelled by the nominal feedforward compensation. The feedback control vector $\delta\underline{u}$ is added to this nominal input $\underline{u}_0$. The feedback control should ensure tracking of the nominal trajectory and should also satisfy the conditions of stability. In order to ascertain whether the system stability is satisfied and to what extend the desired system behaviour is ensured, the tracking behaviour of the complete system must be analyzed through dynamic simulations.

6. Implementation

The perturbation method presented in the previous section is added to our implementation of the finite element program SPACAR [18]. It has interfaces to the MATLAB and SIMULINK [11] environment. In this way a large set of tools for, e.g., data processing, graphical presentation, simulation and control system design are available for dynamic analyzes of flexible manipulators.

Figure 3 shows the block diagram of a typical closed-loop simulation in SIMULINK which is based on the perturbation method. The so-called LTV block in this diagram solves Equation (24). Its input $\delta\underline{u}$ is computed by a controller from the output $\delta\underline{y}$ of the LTV block. This output will be discussed below. Along the nominal trajectory $\delta\underline{y} = 0$ and hence the reference signal for the controller is zero.

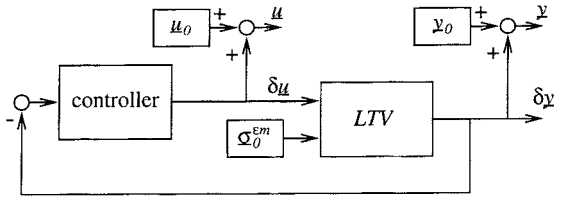

Figure 3. Block diagram of a typical closed-loop simulation in SIMULINK based on the perturbation method.

Within the SIMULINK framework the LTV block represents an *extended* Linear Time-Varying state space system

$$\begin{cases} \dot{\underline{x}}_{\mathrm{ss}} &= A_{\mathrm{ss}}\underline{x}_{\mathrm{ss}} + B_{\mathrm{ss}}\underline{u}_{\mathrm{ss}}, \\ \underline{y}_{\mathrm{ss}} &= C_{\mathrm{ss}}\underline{x}_{\mathrm{ss}} + \dfrac{1}{2}\,(G_{\mathrm{ss}}\cdot\underline{x}_{\mathrm{ss}})\cdot\underline{x}_{\mathrm{ss}}, \end{cases} \tag{26}$$

where $\underline{u}_{\mathrm{ss}}$, $\underline{y}_{\mathrm{ss}}$ and $\underline{x}_{\mathrm{ss}}$ are the input, output and state vectors, respectively, and A_{ss}, B_{ss} and C_{ss} are the time-varying state space matrices. The usual state space representation is supplemented with a second order term in the output equation for $\underline{y}_{\mathrm{ss}}$ which includes a time-varying tensor G_{ss} that will be explained below.

Equation (24) is written in the LTV representation (26) by defining the state and input vectors

$$\underline{x}_{\mathrm{ss}} = \begin{bmatrix} \delta\underline{q} \\ \delta\dot{\underline{q}} \end{bmatrix}, \quad \underline{u}_{\mathrm{ss}} = \begin{bmatrix} \delta\underline{u} \\ \underline{\sigma}_0^{\varepsilon m} \end{bmatrix}. \tag{27}$$

The state space matrices A_{ss} and B_{ss} are then computed with a straightforward procedure from the matrices in Equation (24), resulting in

$$\begin{aligned} A_{\mathrm{ss}} &= \begin{bmatrix} 0 & I \\ -\bar{M}_0^{-1}\bar{K}_0 & -\bar{M}_0^{-1}C_0 \end{bmatrix}, \\ B_{\mathrm{ss}} &= \begin{bmatrix} 0 \\ \bar{M}_0^{-1} \end{bmatrix}. \end{aligned} \tag{28}$$

The output matrix C_{ss} depends on the output vector $\underline{y}_{\mathrm{ss}}$ that is defined by the user. It may consist of (first derivatives of) the degrees of freedom present in $\underline{x}_{\mathrm{ss}}$ or (first derivatives of) coordinates that are computed from $\underline{x}_{\mathrm{ss}}$ using Equation (20). For a highly flexible manipulator with large deformations this linear approximation may be inaccurate. Then higher order terms are added. The quadratic approximation of $\delta\underline{x}$ is

$$\delta\underline{x} = \mathrm{D}\underline{\mathcal{F}}_0\,\delta\underline{q} + \frac{1}{2}(\mathrm{D}^2\underline{\mathcal{F}}_0\cdot\delta\underline{q})\cdot\delta\underline{q}. \tag{29}$$

Figure 4. Elastic beam attached to a hub rotating about an axis fixed in space.

By combining Equation (29) with Equations (26) and (27) the coordinates $\delta\underline{x}$ in $\underline{y}_{ss}$ are computed using

$$C_{ss} = \left[\mathrm{D}\underline{\mathcal{F}}_0 \;\; 0 \right],$$
$$G_{ss} = \begin{bmatrix} \mathrm{D}^2\underline{\mathcal{F}}_0 & 0 \\ 0 & 0 \end{bmatrix}. \tag{30}$$

For the purpose of the trajectory tracking control the total trajectory time T is divided into N intervals. The state space matrices and the vectors $\underline{\sigma}_0^{\varepsilon m}$, $\underline{u}_0$ and $\underline{y}_0$ are computed during a preprocessing run at the discrete time steps $t = t_i$ ($i = 0, 1, 2, ..., N$). During the simulation runs these data are read from files. Between two time steps the coefficients of the state space matrices are interpolated linearly. Cubic interpolation is used for the vectors $\underline{\sigma}_0^{\varepsilon m}$, $\underline{u}_0$ and $\underline{y}_0$.

7. Planar One Link Flexible Manipulator

The perturbation method outlined in this paper has first been tested by means of simulations of a one link flexible manipulator which has been studied by several authors [12, 15, 19–23]. The arm is attached to a hub which is driven by a motor. The arm consists of a slender beam of length $l = 8.0$ m. The beam has a rectangular cross-section of 0.03675 m by 0.001986 m, so the area is $A = 7.3 \cdot 10^{-5}$ m^2 and the area moment of inertia is $I = 8.218 \cdot 10^{-9}$ m^4. It is made of aluminum with density $\rho = 2766.67$ kg/m^3 and Young's modulus $E = 6.895 \cdot 10^{10}$ N/m^2. The hub and the beam are modeled by a cylindrical hinge element and four planar beam elements having equal lengths, as shown in Figure 4. Of each beam element the two bending deformations of Equations (2) are taken into account. The longitudinal deformations of the elements due to normal forces are suppressed. The lateral deflection δy of the tip of the beam is taken as an observed quantity. The linearized equations of motion governing the transverse vibrations of the elastic beam rotating about an axis fixed in space are given by

$$\begin{bmatrix} \bar{m}_0^{ee} & \bar{M}_0^{e\varepsilon} \\ \bar{M}_0^{\varepsilon e} & \bar{M}_0^{\varepsilon\varepsilon} \end{bmatrix} \begin{bmatrix} \delta\ddot{e}^m \\ \underline{\ddot{\varepsilon}}^m \end{bmatrix} + \begin{bmatrix} 0 & 0 \\ 0 & \bar{K}_0^{\varepsilon\varepsilon} \end{bmatrix} \begin{bmatrix} \delta e^m \\ \underline{\varepsilon}^m \end{bmatrix} = \begin{bmatrix} -\delta\sigma^{em} \\ \underline{\sigma}_0^{\varepsilon m} \end{bmatrix}, \tag{31}$$

in which e^m is the relative rotation angle of the hinge, $\underline{\varepsilon}^m$ is the vector of the eight flexible deformation coordinates and $\bar{m}_0^{ee} = \rho A l^3/3$ is the mass moment of inertia of the rigid beam about the hinge point. According to definition (25) the stiffness

$\bar{K}_0^{\varepsilon\varepsilon}$ includes the matrices $N_0^{\varepsilon\varepsilon}$ and $G_0^{\varepsilon\varepsilon}$ that are symmetric matrices and may be viewed as additional centrifugal stiffening matrices. In this example matrix C_0 is zero.

7.1. CONSTRAINED MOTION

The constrained motion of the manipulator is obtained when the input angle e^m is prescribed as function of time, i.e. $\delta e^m(t) = 0$. Then the flexible motion of the system is described by

$$\bar{M}_0^{\varepsilon\varepsilon}\,\underline{\ddot{\varepsilon}}^m + \bar{K}_0^{\varepsilon\varepsilon}\,\underline{\varepsilon}^m = \underline{\sigma}_0^{\varepsilon m}. \tag{32}$$

The associated frequency equation is given by

$$\det(-\omega_i^2 \bar{M}_0^{\varepsilon\varepsilon} + \bar{K}_0^{\varepsilon\varepsilon}) = 0, \tag{33}$$

where ω_i are the natural frequencies of the constrained modes.

We consider the particular case in which the beam is accelerated from rest to a constant angular velocity. The prescribed angle of rotation e^m is given by

$$e^m(t) = \begin{cases} 0, & t < 0, \\ \dfrac{\Omega}{T}\left[\dfrac{1}{2}t^2 + \dfrac{T^2}{4\pi^2}\left(\cos\dfrac{2\pi t}{T} - 1\right)\right], & 0 \le t \le T, \\ \Omega\left(t - \dfrac{1}{2}T\right), & t > T. \end{cases} \tag{34}$$

The final angular velocity $\Omega = 4$ rad/s and the spin-up time $T = 15$ s. The beam may be considered as a clamped-free beam.

Figure 5 shows the tip deflection δy computed by means of the perturbation method for five different cases:

case 1:	Equation (32),	full linearized model including all stiffness terms,
case 2:	idem,	quasi-static solution using $(K_0^{\varepsilon\varepsilon} + N_0^{\varepsilon\varepsilon} + G_0^{\varepsilon\varepsilon})\underline{\varepsilon}^m$,
case 3:	idem,	neglecting the stiffening terms $N_0^{\varepsilon\varepsilon}\underline{\varepsilon}^m$ and $G_0^{\varepsilon\varepsilon}\underline{\varepsilon}^m$,
case 4:	idem,	quasi-static solution using only $K_0^{\varepsilon\varepsilon}\underline{\varepsilon}^m$,
case 5:	idem,	neglecting the geometric stiffening term $G_0^{\varepsilon\varepsilon}\underline{\varepsilon}^m$.

To evaluate the perturbation solution the number of linearization points used is increased in the numerical simulations until the solution converges to the non-linear solution of Equation (13). Using too few linearization points may cause an unphysical excitation of a natural frequency. When the number of linearization points is increased to 60, no differences can be observed between the non-linear and the perturbation solution (case 1) at the presented scale. The results shown in Figure 5 are computed using 600 linearization points.

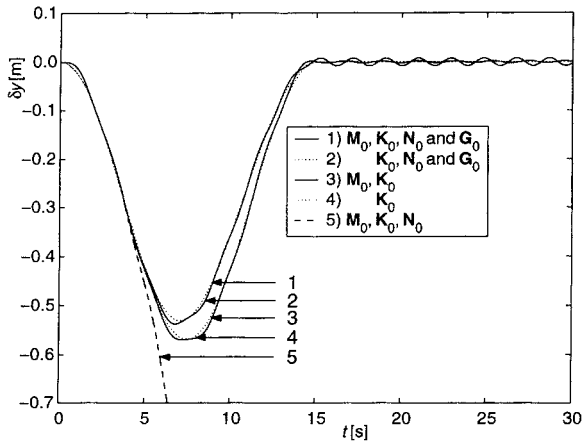

Figure 5. Tip-deflection δy for spin-up motion using different perturbation approximations.

Table I. Comparison of the results from different calculations of the maximum deflection of the tip of the beam.

Model	number of elements	Max. deflection [m]
SPACAR, non-linear [15]	4	0.536
Wu and Haug [19]	4 substructures	0.556
idem	6 substructures	0.543
perturbation, case 1	4	0.537
idem, case 2	4	0.531
idem, case 3	4	0.569
idem, case 4	4	0.569
idem, case 5	4	∞

The values of the maximum deflection obtained from the different (perturbation) approximations and non-linear simulations are listed in Table I and confirm quantitatively the behaviour shown in Figure 5. Using the quasi-static equations, including all stiffening terms (case 2), we obtain results of comparable accuracy as obtained with the full linearized equations. However, when only the geometric non-linear stiffening term $G_0^{\varepsilon\varepsilon}\underline{\varepsilon}^m$ is cancelled (case 5), the solution diverges as the spin rate approximates the natural frequency of the first bending mode. This can also be observed from a change in the natural bending frequency of the beam.

Figure 6 shows the time histories of the natural frequencies of the first constrained bending mode, defined by Equation (33) for the cases 1 and 5, respectively. This figure shows that the first natural frequency for case 1 increases from 2.91 to 3.27 rad/s. The initial value agrees with the analytical value for a clamped-free beam [24]. However, when the geometric stiffening term $G_0^{\varepsilon\varepsilon}\underline{\varepsilon}^m$ has been neglected

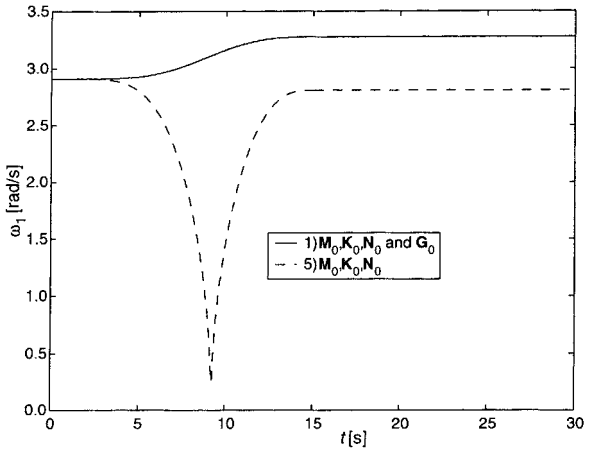

Figure 6. Time dependent natural frequency ω_1 of the first constrained bending mode.

(case 5) a zero first natural frequency is calculated as the spin-up rate approximates the natural frequency of the first bending mode. Furthermore, it appears from Figure 6 that the stress stiffening terms associated with the dynamic stiffening matrix $N_0^{\varepsilon\varepsilon}$ and the geometric stiffening matrix $G_0^{\varepsilon\varepsilon}$ nearly cancel.

Note that a simple linearized model (case 3) in which both the dynamic and geometric stiffening terms are neglected yields a stable solution. If we compare the results for cases 3 and 4 with those from case 1, we observe that the maximum deflection is only 6% larger. This is in contradiction with results obtained by Wu and Haug [19] who obtained an unbounded solution with their linear model (no account for stiffening effects).

7.2. CONTROLLED TRAJECTORY MOTION

Controlled trajectory motion is studied in a numerical example in which the beam shown in Figure 4 is driven 90° counterclockwise in a rest-to-rest maneuver by a torque actuator located at the hinge. The desired hub angular position profile is given by

$$e_0^m(t) = \begin{cases} 0, & t < 0, \\ \dfrac{\pi}{2}\dfrac{t}{T} - \dfrac{1}{4}\sin\left(\dfrac{2\pi t}{T}\right), & 0 \le t \le T, \\ \dfrac{\pi}{2}, & t > T, \end{cases} \tag{35}$$

where $T = 5$ s is the desired maneuver time. The torque is governed by a control algorithm consisting of an open-loop and a closed-loop component. The required open-loop torque u_0 is calculated with Equation (23). For the presented case the open-loop torque is expressed as $u_0 = \bar{m}_0^{ee}\ddot{e}_0^m$. Proportional plus derivative joint

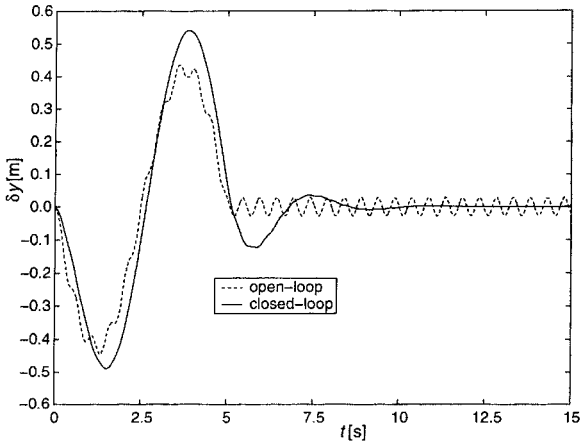

Figure 7. Tip-deflection δy using the perturbation method for a trajectory motion without controller (open-loop) and for controlled trajectory motion (closed-loop with $\omega = 1.45$ rad/s and $\beta = 0.9$ in Equation (37)).

feedback is used in which the position sensors are collocated with the actuators. The control law is given by

$$\delta u = -k_p \delta e^m - k_v \delta \dot{e}^m \tag{36}$$

where k_p and k_v are the angular position and angular rate feedback gains. This feedback control law has a structure which is based on the rigid link model of the manipulator while the determination of the control gains is based on a model which includes the flexible behaviour of the manipulator arm. The feedback gains are specified by Book et al. [25]

$$\begin{aligned} k_p &= \bar{m}_0^{ee} \omega^2, \\ k_v &= 2\bar{m}_0^{ee} \beta \omega, \end{aligned} \tag{37}$$

where ω and β are the desired servo loop frequency and the corresponding active damping ratio. To obtain adequate damping of the lowest flexible mode, a bandwidth of approximately $\omega = 0.5\omega_1$ and a relative damping $\beta = 0.7 \ldots 0.9$ suffices, where ω_1 is the lowest constrained natural frequency according to Equation (33).

The trajectory has been computed with the perturbation method taking 600 linearization points as before. Figure 7 shows the tip-deflection δy for the controlled trajectory motion in comparison with an uncontrolled motion (open-loop, i.e. only feedforward). In both cases differences between the non-linear and the perturbation solutions are smaller than $5 \cdot 10^{-4}$ m, which is too small to be observed at the presented scale. The simulation shows clearly that the designed controller damps the natural oscillation and stabilizes the motion.

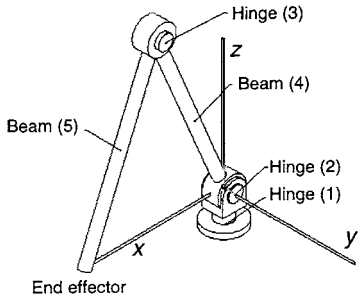

Figure 8. Spatial two link manipulator.

Table II. Kinematic and dynamic link parameters.

Beam number	4	5
Length l (m)	0.7	0.7
Bending stiffness EI/l^3 (N/m)	48300	24460
Torsion stiffness GI_p/l^3 (N/m)	41580	∞
Mass per unit length m (kg/m)	4	2

8. Spatial Two Link Flexible Manipulator

To investigate the applicability of the perturbation method a more complex manipulator will be studied next. This is a spatial two link flexible manipulator moving in a gravitational field. Figure 8 illustrates the finite element representation of this manipulator. The revolute joints of the manipulator are modeled by the hinge elements (1), (2) and (3). The rotational axes of the hinge elements (2) and (3) are parallel, thus providing the in-plane motion of the manipulator. The manipulator can rotate relative to the inertial reference frame (x, y, z) about the vertical axis of hinge (1), which coincides with the z axis of the reference frame. The hinges are driven by internal actuators, which are modeled as pure torque sources without dynamics. The two links of the manipulator, modeled by beam elements (4) and (5), are respectively referred to as upper arm and forearm. Both arms have uniform cross sections and are assumed to be flexible. The longitudinal deformation in both arms and the torsional deformation in the forearm are suppressed. Referring to Figure 8, Table II lists the other kinematic and dynamic properties of the links. The masses of the bearing assembly at the elbow hinge (3) and of the end effector are modeled by point masses of 10 and 30 kg, respectively. The gravity loads, including the loads due to the distributed mass of the links, are taken into account by applying the corresponding external forces in the negative z direction. The corresponding model has nine flexible degrees of freedom in addition to the actuator joint coordinates e_1, e_2 and e_3 representing the relative rotations of the actuators.

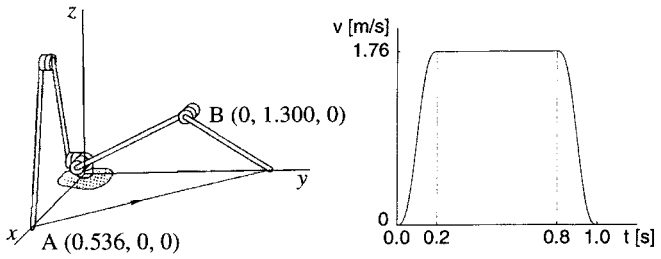

Figure 9. Motion trajectory and velocity profile of manipulator tip.

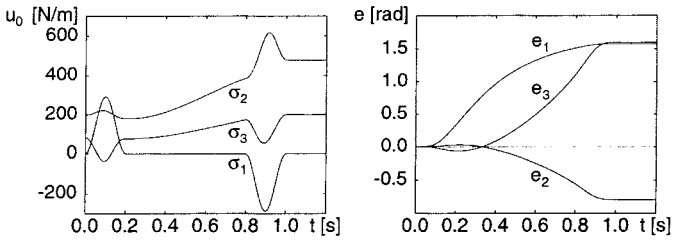

Figure 10. Nominal actuator moments applied at hinges (1), (2) and (3) and the nominal relative rotations of the hinges. The rotations e_1, e_2 and e_3 are relative to their initial positions.

The manipulation task implies transferring the manipulator tip along a straight line with a smooth velocity profile, see Figure 9. The initial and final manipulator configurations are given by the configurations A and B. The acceleration and deceleration in the velocity profile is composed of squared sines.

Solving the inverse kinematic and dynamic problem yields the actuator rotations and the necessary actuator moments (Figure 10). It is obvious, that even for a relative simple trajectory (straight line) of the manipulator tip, rather complicated setpoint functions for the actuators are needed. Furthermore, the motion of the manipulator is not stable if no controller is used and only the nominal moments of Figure 10 are applied. That means that even a small deviation from the nominal path will lead to a completely different trajectory. Hence, in the remaining part of this section only controlled trajectory motion will be studied.

8.1. CONTROLLED TRAJECTORY MOTION

The same control strategy will be applied as has been described in Section 7.2 for the one link manipulator. With proportional position and velocity joint feedback the control law is

$$\delta \underline{u} = -K_p \delta \underline{e}^m - K_v \delta \underline{\dot{e}}^m. \tag{38}$$

This manipulator is a MIMO system, so in comparison with Equation (36) the control input $\delta \underline{u}$ is a vector and K_p and the K_v are matrices containing nine gains each, instead of one single gain used for the one link manipulator. The gain matrices

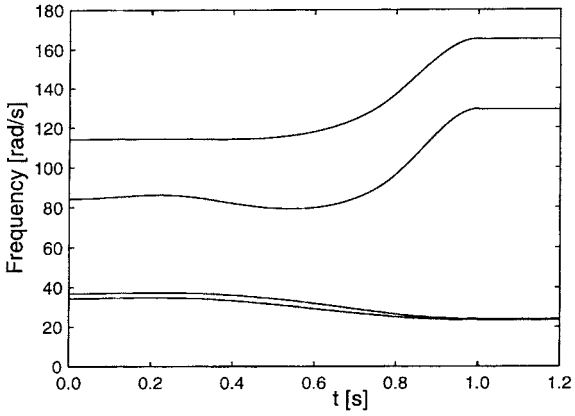

Figure 11. Four lowest constrained natural frequencies during the manipulator motion.

K_p and K_v are given by

$$\begin{aligned} K_p &= \bar{M}_0^{ee}\Omega^2, \\ K_v &= 2\bar{M}_0^{ee}\beta\Omega, \end{aligned} \tag{39}$$

where

$$\Omega = \begin{bmatrix} \omega_1 & & 0 \\ & \omega_2 & \\ 0 & & \omega_3 \end{bmatrix} \quad \text{and} \quad \beta = \begin{bmatrix} \beta_1 & & 0 \\ & \beta_2 & \\ 0 & & \beta_3 \end{bmatrix}, \tag{40}$$

are the desired servo loop frequencies and active damping ratios, respectively. The frequencies ω_i can be tuned to the lowest constrained natural frequencies of the corresponding in-plane and out-of-plane motion. The natural frequencies are computed with the frequency equation (33).

While moving along the trajectory, the natural frequencies of the manipulator will chance due to the changing configuration. Figure 11 shows the four lowest constrained natural frequencies as functions of the time t. Obviously, the natural frequencies change gradually with respect to the manipulator configuration. The corresponding mode shapes are determined for the initial and the final configuration, see Figure 12. Furthermore, the inertia properties depend on the configuration, so the mass matrix $\bar{M}_0^{ee}$ in Equation (39) will also change during the simulation. To simplify the control algorithm only the mass matrix $\bar{M}_0^{ee}$ is updated and a constant magnitude for the servo loop frequencies is used that is half of the lowest natural frequency during the complete motion. In our simulations $\omega_i = 11.8$ rad/s and $\beta_i = 0.85$ have been used.

The simulations have been carried out using the non-linear finite element method and using the perturbation method with several number of linearization points. Figure 13 shows the deviation from the nominal trajectory for the manipulator tip. The results are plotted according to a non-linear simulation and from two simulations

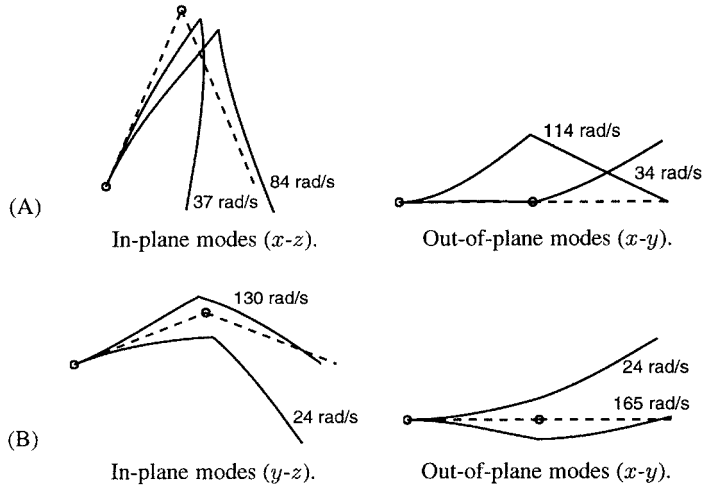

Figure 12. Constrained mode shapes in initial (A) and final (B) configurations.

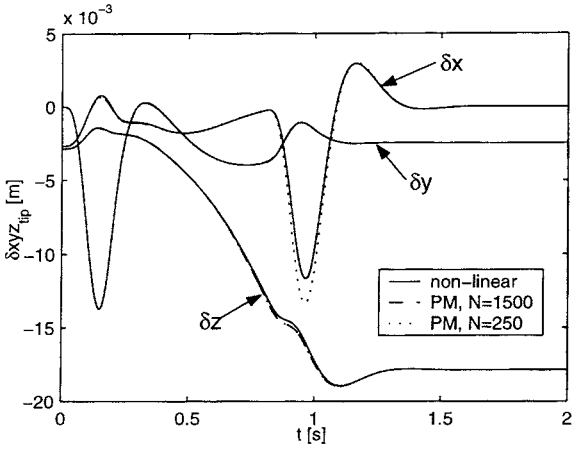

Figure 13. Deviation from the nominal tip trajectory according to a non-linear simulation and from the perturbation method (PM) using 250 and 1500 linearization points N, respectively.

with the perturbation method using 250 and 1500 linearization points, respectively. In all simulations the manipulator is at rest at $t = 0$ s. The deformations of the links are computed by determining the steady solution of the linearized equation of motion (24)

$$\bar{K}_0 \begin{bmatrix} \delta \underline{e}^m \\ \underline{\varepsilon}^m \end{bmatrix} = \begin{bmatrix} \delta \underline{u} \\ \underline{\sigma}_0^{\varepsilon m} \end{bmatrix}, \tag{41}$$

where $\delta \underline{u}$ satisfies Equation (38) with $\delta \dot{\underline{e}}^m = \underline{0}$. In the solution of Equation (41) e_2, e_3 and bending deformations in $\underline{\varepsilon}^m$ are non-zero due to the gravity. The bending of the manipulator in the xz-plane is clearly expressed by the non-zero δx_{tip} and δz_{tip} at $t = 0$ s in Figure 13. The steady solution of the linearized equation of

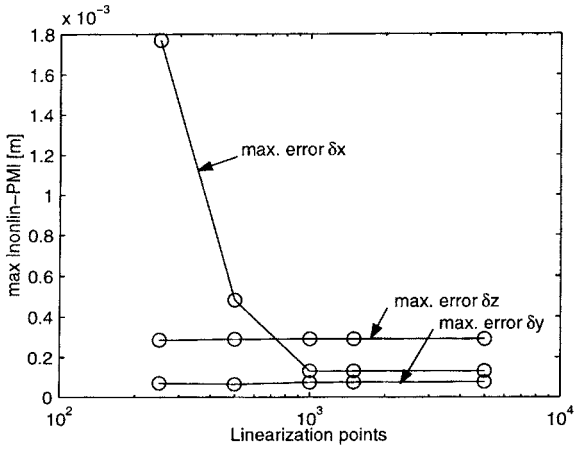

Figure 14. Maximum errors in the coordinates of the tip position as functions of the number of linearization points. The error is defined as the difference in each coordinate between the perturbation method (PM) and the non-linear simulation.

motion according to Equation (41) is also used in the non-linear simulations. Due to non-linear effects the true steady solution of the non-linear equation of motion is different, but this difference is small and will be neglected.

For 0 s $< t <$ 1 s the manipulator moves along the trajectory. The effects of acceleration and deceleration can be seen in Figure 13. Clearly, all simulations show that the proposed controller is stable and the manipulator is practically at rest for $t >$ 1.5 s. Now the bending of the manipulator in the yz-plane results in non-zero δy_{tip} and δz_{tip}. Obviously, the deviation in the z direction is larger than at $t = 0$ s as the distance of the tip of the manipulator to the origin is larger.

Some differences are found in the simulations of Figure 13. The z position for $t \approx 0.85$ s is slightly lower according to the perturbation method than the non-linear result. Using more linearization points does not improve the agreement. Near $t = 1$ s the x position according to the perturbation method depends strongly on the number of linearization points. The simulation with 1500 linearization points can not be distinguished from the non-linear simulation in Figure 13. With only 250 linearization points clearly a larger discrepancy is found.

These effects are summarized in Figure 14 where for each coordinate the maximum error along the trajectory is plotted as a function of the number of linearization points. The x coordinate clearly depends on the number of linearization points. Below 1000 linearization points there is a discrepancy as illustrated in Figure 13. Using more linearization points the maximum error is found near 0.15 s and is hardly visible in Figure 13. For the y and z coordinates some small differences are found, which do not change in the range from 250 to 5000 linearization points.

9. Conclusions

The presented perturbation method proved to be an efficient tool for numerical simulation of flexible manipulator analysis. For the flexible one link manipulator, results of the perturbation method agree well with the results obtained from a full non-linear analysis. An essential prerequisite for this perturbation method is the availability of accurate linearized equations.

Closed-loop behaviour is efficiently and accurately simulated within the presented framework. The simulation of a more complex spatial manipulator showed also a good agreement between the perturbation method and the non-linear analysis, provided that sufficient linearization points are used.

Acknowledgement

The authors acknowledge the work carried out by R.R. Waiboer and H. Super on the implementation and simulations of the perturbation method.

References

1. Winfrey, R.C., 'Elastic link mechanism dynamics', *J. Engrg. Indust.* **93**, 1971, 268–272.
2. Erdman, A.G., Sandor, G.N. and Oakberg, R.G., 'A general method for kineto-elastodynamic analysis of mechanisms', *J. Engrg. Indust.* **94**, 1972, 1193–1205.
3. Imam, I., Sandor, G.N. and Kramer, S.N., 'Deflection and stress analysis in high speed planar mechanisms with elastic link', *J. Engrg. Indust.* **95**, 1973, 541–548.
4. Cleghorn, W.L., Fenton, R.G. and Tabarrok, B., 'Finite element analysis of high speed flexible mechanisms', *Mech. Mach. Theory* **16**, 1981, 407–424.
5. Sunada, W.H. and Dubowsky, S., 'On the dynamic analysis and behavior of industrial robot manipulators with elastic members', *J. Mech. Transmissions Automat. Design* **105**, 1983, 42–51.
6. Turcic, D.A. and Midha, A., 'Dynamic analysis of elastic mechanism systems. Part I: Applications', *J. Dynam. Systems Meas. Control* **106**, 1984, 249–254.
7. Turcic, D.A., Midha, A. and Bosnik, J.R., 'Dynamic analysis of elastic mechanism systems. Part II: Experimental results', *J. Dynam. Systems Meas. Control* **106**, 1984, 255–260.
8. Siciliano, B. and Book, W.J., 'A singular perturbation approach to control of lightweight flexible manipulators', *Internat. J. Robotics Res.* **7**, 1988, 79–90.
9. Schwab, A.L. and Meijaard, J.P., 'Small vibrations superimposed on non-linear rigid body motion', in *Proceedings of DETC'97, 1997 ASME Design Engineering Technical Conferences*, Sacramento, CA, September 14–17, ASME, New York, 1997, 1–7.
10. Jonker, J.B. and Meijaard, J.P., 'SPACAR-computer program for dynamic analysis of flexible spatial mechanisms and manipulators', in *Multibody Systems Handbook*, W. Schiehlen (ed.), Springer-Verlag, Berlin, 1990, 123–143.
11. SIMULINK, *Dynamic System Simulation for* MATLAB*, Using* SIMULINK *Version 3*, The MathWorks Inc., Natick, MA, 1999.
12. Kane, T.R., Ryan, R.R. and Banerjee, A.K., 'Dynamics of a cantilever beam attached to a moving base', *J. Guidance Control Dynam.* **10**, 1987, 139–151.
13. Visser, W. and Besseling, J.F., 'Large displacement analysis of beams', Report WTHD-10, Laboratory for Engineering Mechanics, Delft University of Technology, 1969.

14. Jonker, J.B., 'A finite element dynamic analysis of flexible manipulators', *Internat. J. Robotics Res.* **9**, 1990, 59–74.
15. Meijaard, J.P., 'Validation of flexible beam elements in dynamics programs', *Nonlinear Dynam.* **9**, 1996, 21–36.
16. Meijaard, J.P., 'Direct determination of periodic solutions of the dynamical equations of flexible mechanisms and manipulators', *Internat. J. Numer. Methods Engrg.* **32**, 1991, 1691–1710.
17. Jonker, J.B., 'Linearization of dynamic equations of flexible mechanisms – A finite element approach', *Internat. J. Numer. Methods Engrg.* **31**, 1991, 1375–1392.
18. Jonker, J.B. and Aarts, R.G.K.M., 'Modelling of flexible mechanisms and manipulators for control purposes', in *Proceedings of the Fourth International Conference on Motion and Vibration Control, MoViC*, Vol. 1, G. Schweitzer, R. Siegwart and P. Cattin (eds), Institute of Robotics, ETH-Zurich, 1998, 291–297.
19. Wu, S.-C. and Haug, E.J., 'Geometric non-linear substructuring for dynamics of flexible mechanical systems', *Internat. J. Numer. Methods Engrg.* **26**, 1988, 2211–2226.
20. Banerjee, A.K. and Dickens, J.M., 'Dynamics of an arbitrary flexible body in large rotation and translation', *J. Guidance Control Dynam.* **13**, 1990, 221–227.
21. Boutaghou, Z.E. and Erdman, A.G., 'A unified approach for the dynamics of beams undergoing arbitrary spatial motion', *J. Vib. Acoust.* **113**, 1991, 495–502.
22. Ryu, J., Kim, S.S. and Kim, S.S., 'A general approach to stress stiffening effects on flexible multibody dynamic systems', *Mech. Struct. Mach.* **22**, 1994, 157–180.
23. Mayo, J. and Dominguez, J., 'A finite element geometrically nonlinear dynamic formulation of flexible multibody systems using a new displacements representation', *J. Vib. Acoust.* **119**, 1997, 573–581.
24. Meirovitch, L., *Elements of Vibration Analysis*, McGraw-Hill, New York, 1970.
25. Book, W.J., Maizza-Neto, O. and Withney, D.E., 'Feedback control of two beam, two joint systems with distributed flexibility', *J. Dynam. Systems Meas. Control* **97**, 1975, 424–431.